A Clustering Analysis of the Morphology of the 130 GeV Gamma-Ray Feature

Eric Carlson[1], Tim Linden[1], Stefano Profumo[1,2] and Christoph Weniger[3]
[1] *Department of Physics, University of California, Santa Cruz, 1156 High Street, Santa Cruz, CA, 95064*
[2] *Santa Cruz Institute for Particle Physics, University of California, Santa Cruz, 1156 High Street, Santa Cruz, CA, 95064 and*
[3] *GRAPPA Institute, University of Amsterdam, Science Park 904, 1090 GL Amsterdam, Netherlands*

Recent observations indicating the existence of a monochromatic γ-ray line with energy $\sim$130 GeV in the Fermi-LAT data have attracted great interest due to the possibility that the line feature stems from the annihilation of dark matter particles. Many studies examining the robustness of the putative line-signal have concentrated on its spectral attributes. Here, we study the morphological features of the γ-ray line photons, which can be used to differentiate a putative dark matter signal from astrophysical backgrounds or instrumental artifacts. Photons stemming from dark matter annihilation will produce events tracing a specific morphology, with a statistical clustering that can be calculated based on models of the dark matter density profile in the inner Galaxy. We apply the DBSCAN clustering algorithm to Fermi γ-ray data, and show that we can rule out the possibility that 1 (2, 4) or fewer point-like sources produce the observed morphology for the line photons at a 99% (95%, 90%) confidence level. Our study strongly disfavors the main astrophysical background envisioned to produce a line feature at energies above 100 GeV: cold pulsar winds. It is highly unlikely that 4 or more such objects have exactly the same monochromatic cosmic-ray energy needed to produce a γ-ray line, to within instrumental energy resolution. Furthermore, we show that the larger photon statistics expected with Air Cherenkov Telescopes such as H.E.S.S.-II will allow for extraordinarily stringent morphological tests of the origin of the "line photons".

PACS numbers: 98.70.Rz, 95.55.Ka, 95.35.+d, 97.60.Gb

I. INTRODUCTION

The launch of the Fermi Large Area Telescope (LAT) in 2008 has allowed for a greatly expanded view of the γ-ray sky, including a significantly enhanced energy and angular resolution, compared to previous missions [1]. These characteristics have allowed, in particular, for a thorough investigation of the extremely dense population of high-energy γ-ray sources in the Galactic center (GC) region [2]. The GC region is known to host such diverse γ-ray sources as supernova remnants [3], highly ionized gas [4], dense molecular clouds [5], massive O/B stars [6], both young and recycled pulsar populations [7], as well as being the densest region of dark matter in the Galaxy [8]. Notably, no other location in the sky is expected to provide a signal from dark matter annihilation which is as bright as the GC (for a recent general review of gamma-ray searches for signals from dark matter annihilation see Ref. [9]). While this makes the GC region an extremely interesting location for a multitude of scientific studies, it also means that additional information, such as characteristic spectra for each source class, must be carefully considered in order to separate the desired signal from the bright background.

Recently, Bringmann et al. [10] and Weniger [11] found indications for a unique spectral signature in observations of the region surrounding the GC, which is consistent with dark matter annihilation. Specifically, in sky regions optimized for large signal-to-noise ratios for various dark matter density profiles, they observed an excess of photons with an energy spectrum resembling a 130 GeV γ-ray line, smeared by the finite energy resolution of the Fermi-LAT telescope. The significance of this excess was found to be 3.2σ globally [11] – enough to make the feature interesting on statistical grounds. The feature is strongest when using regions of interest that have been optimized for dark matter density distributions following: (1) a Navarro-Frenk-White (NFW) profile [12], (2) an Einasto profile [13], and (3) a generalized NFW profile, with a radial slope governing the dark matter density profile ($\mathrm{r}^{-\alpha}$) set to $\alpha = 1.15$, similar to what could result from adiabatic contraction [14, 15]. The reported feature is much weaker for profiles where the dark matter density is cored near the GC.

A monochromatic γ-ray line has been long considered the "Holy Grail" for dark matter indirect detection, given the difficulty of producing a high-energy monochromatic signal with ordinary astrophysical processes. Thus, this observation prompted a number of follow-ups. Profumo and Linden [16] noted that the observation of a monochromatic γ-ray signal could be qualitatively mimicked by an additional power-law component which breaks strongly at an energy of 130 GeV, and posited the Fermi bubbles [17] as a possible source for this excess (although rather strong breaks are required to fit the data, see Ref. [9]). Most notably, Su and Finkbeiner [18] localized the emission to within approximately 5° of the GC, finding a 6.5σ (5.0σ after including a trials factor) preference for a line signal following an off-center Einasto profile compared to the assumption of a simple power-law background (see also [19]). This finding disputes the implication of the Fermi bubbles as a source for the excess, as the latter are observed to extend over a

much larger emission region. The off-centered nature of the dark matter profile is at the moment only marginally statistically significant [20, 21]. However, if confirmed, an off-center peak would pose a challenge to traditional models of the Galactic dark matter density which assume the largest dark matter density to fall on top of the peak of the baryonic mass density[1]. However, a recent analysis by Kuhlen et al. [22] found that the peak in the dark matter density may, in fact, be displaced by hundreds of parsecs from the dynamical center of the Galaxy - although this scenario might be incompatible with the assumption of a cusped profile.

More data are needed to clarify whether the 130 GeV feature in the data persists with larger statistics or if it is only a statistical fluke. Since the observation of a γ-ray line is extremely sensitive to inaccuracies in the energy-reconstruction of γ-rays observed by Fermi-LAT, a great deal of interest has also focused on searching for possible instrumental abnormalities affecting the photons belonging to the γ-ray line. The most notable characteristic of any such instrumental effect would be the observation of line activity either across the entire sky, or across a certain region of instrumental phase space. Interestingly, some early results found an excess of 130 GeV events in observations of the Earth-limb [18, 23, 24]. This is troubling, as the vast majority of limb photons are known to result from the di-photon π^0 decay spectrum created as cosmic-ray protons interact with the upper layers of the Earth's atmosphere. There is no conceivable model in which dark matter annihilation could create a γ-ray line in this region [18]. However, this line activity was not detected along the Galactic plane, which provides significantly more photons than the GC, and inhabits similar regions of instrumental phase space. A comprehensive study by Finkbeiner et al. [23] did not find any significant evidence for systematic features in the energy reconstruction of the Fermi-LAT, which would be able to artificially produce a γ-ray line (see however Refs. [25–27]).

Follow up analyses by the Fermi-LAT team are currently ongoing, but have revealed two noteworthy results. At the time of the initial discovery of the γ-ray line, efforts were already ongoing to improve the energy normalization of the Fermi-LAT data, accounting for a decrease in the calculated energy of γ-rays over time due to radiation damage to the calorimeter. This effect linearly increased the reconstructed energy of high energy photons, moving the line signal from 130 GeV up to approximately 135 GeV. However, this reprocessing did not greatly affect any other signature of the posited line analysis. We note that throughout the rest of this paper, we refer to the "130 GeV line", as we are using a version of the Fermi-LAT data which has not been reprocessed. However, all results shown here are very nearly applicable to an analysis of the 135 GeV line observed in the reprocessed data.

Additionally, the Fermi-LAT analysis did uncover one troubling aspect of the posited γ-ray line. Employing a parameter CTBBestEnergyProb (which is not publicly available), they investigated the confidence they had in the energy reconstruction of each photon belonging to the γ-ray line. In the case where a true γ-ray line feature is present in the data, this should increase the statistical significance of the observation, as the proceedure adds additional statistical weight to the line photons which are most likely to have a correctly measured energy. However, when this analysis was applied to the observed photon data, the statistical significance of the line feature was found to decrease moderately. This signals that the line feature has photons with a somewhat poorer energy resolution than would generally be expected[28]. However, further inquiry of these systematic issues is required, as none of the systematics can clearly account for the entire statistical strength of the line feature.

If interpreted as a signal of particle dark matter annihilation or decay, the large observed intensity of the 130 GeV γ-ray line (along with strong constraints on the total continuum emission from additional hadronic states [29]) has proved a difficult, though by no means intractable, particle physics problem. Numerous models have already been posited to "brighten" the γ-ray line [30–59]. Summarizing the myriad particle physics details of these models lies beyond the scope of the present paper.

Although often characterized as a "smoking gun" signature for the annihilation or decay of particle dark matter, tentative observations of the 130 GeV line have spurred the question of whether any traditional astrophysical mechanism might mimic a line in the relevant energy range. Aharonian et al. [60] argued that the only plausible mechanism for the creation of an astrophysical γ-ray line is through inverse Compton scattering of ambient photons by a jet of nearly monoenergetic electrons and/or positrons, occurring in the deep Klein-Nishina regime. If the latter kinematic regime holds, the photon acquires nearly the entire energy of the incoming lepton, allowing for a nearly monoenergetic lepton spectrum to efficiently transfer into a sharply peaked γ-ray feature.

One possible class of astrophysical objects that possesses the potential to host the needed leptonic monochromatic "jet", as well as the ambient photons in the needed energy range (here, a few eV) is *cold ultra-relativistic pulsar* (PSR) *winds* [60]. It is important to note that this scenario presents a potential difficulty in explaining the observed spread of 130 GeV photons beyond a single point source, as different PSRs would be expected to exhibit γ-ray lines at different energies. One way to test this one astrophysical background is therefore to study whether the morphology of the observed 130 GeV photons can be reproduced with a small number of point sources or not. This is the key objective of the present study.

[1] Which we assume, here, to be identical to the position of Sgr A*, and call the GC throughout this paper.

Several other approaches have tested the dark matter nature of the 130 GeV photons. For example, any dark matter interpretation of the 130 GeV line implies additional regions of interest for follow up searches, where the so-called J-factor (the line-of-sight integral of the dark matter density squared, smeared over the instrumental point-spread function) is expected to be largest. Most importantly, dwarf spheroidal galaxies and galaxy clusters have been singled out as promising regions to search for a dark matter signal. Observations of Milky Way dwarfs have not uncovered any evidence of a 130 GeV signal [61]: this is not unexpected, as the estimated annihilation cross-section to $\gamma\gamma$ implied from GC observations predicts less than one photon to arrive from the population of dwarf spheroidal galaxies. Interestingly, Hektor et al. [62] argued for an observation of a 130 GeV line in a population of nearby galaxy clusters. However, it should be noted that this signature is only significant when very large ROIs of $\sim 8^\circ$ are considered, which is much larger than the expected angular size of the galaxy clusters under investigation.

Using a similar method, Su and Finkbeiner [63] investigated the population of unassociated Fermi-LAT point sources – that is, point sources detected by the Fermi-LAT instrument which have not been identified at other wavelengths. They found a statistically significant detection for a double 130 GeV and 111 GeV line, with 14 unassociated sources showing evidence of a line photon. Furthermore, they found no significant detection of γ-ray line emission in the control sample of Fermi-LAT point sources that have already been associated with various astrophysical phenomena. This caused them to conclude that some portion of the unassociated point-source sample may contain previously unknown dark matter substructures. However, Hooper and Linden [64] argue against this conclusion, noting that each unassociated source is identified primarily based on its continuum emission between energies of 100 MeV-10 GeV, rather than based on the detection of a single line photon. The intensity and spectrum of this continuum emission can then be compared to the signal from dark matter annihilation to any final state producing a γ-ray continuum, and is expected in order to produce the thermal relic abundance of dark matter. They find that for at least 12 of the 14 indicated unassociated point sources, the continuum emission is not compatible with any dark matter annihilation pathway. Furthermore, they argue that the latitude distribution of the identified sources is not consistent with that expected from any model of dark matter subhalo formation. A second analysis by Mirabal [65] argued that while these 14 sources remain unidentified, at least 12 of the sources (not identical to those from [64]) are spectrally strongly consistent with AGNs.

In addition to considering the energy signature of the 130 GeV line, understanding the morphology of the photons belonging to the source class producing the observed feature will be key to elucidate the physics behind the line phenomenon. Notably, the point-spread function of front-converting events at energies near 100 GeV approaches 0.1° [1], which is significantly smaller than the $\sim 5^\circ$ region of interest implicated by [18], allowing for the actual morphology of the line emission to be closely mirrored by Fermi-LAT observations. To first order, observations indicating a morphology consistent with widely accepted dark matter density profiles would provide additional evidence for a dark matter interpretation (the data indeed points to that direction, see e.g. Fig. 3 of Ref. [9]), while measurements consistent with either a population of point sources, or a significantly flattened profile may point to other astrophysical or instrumental interpretations.

In this *paper*, we examine the morphology of photons belonging to the γ-ray line more closely, analyzing with a sound statistical approach the distribution of the arrival direction of photons by employing a clustering algorithm to pinpoint the correlation between the arrival directions of photons putatively belonging to the line feature. We then compare these results against simulated models where the line is produced by dark matter annihilation or by an astrophysical process associated with a few point sources (for example a handful of PSRs). The key result of our study is that *current data disfavor a scenario where the line photons stem from 4 or fewer point sources*. Given how unlikely it is that 4 or more pulsars produce a gamma-ray line at exactly the same energy (within the LAT energy resolution), our study disfavors the PSR scenario over a truly diffuse and un-clustered origin for the photons.

In Section II we describe the data employed in our observations of the γ-ray line feature, the specifics of the algorithms used to determine the photon morphology, our models for both the annihilation of dark matter and emission from PSRs, and the diffuse background in the region. In Section III we present the results of our study both for current Fermi observations, and for projections for upcoming observations of the GC with the Atmospheric Cherenkov Telescope (ACT) H.E.S.S.-II. Finally, in Section IV we discuss the interpretation of the results, and present our conclusions.

II. MODELS

A. Photon Selection

In order to analyze the population of photons stemming from the putative γ-ray line emission, we must make a photon selection which isolates the line photons from those correlating to background events. We follow here the same photon selection employed in Ref. [66], which provides the location of observed Fermi-LAT photons in three energy bands, 70-110 GeV, 120-140 GeV, and 150-300 GeV over a 10° square window centered on the GC. Since the Fermi-LAT energy resolution is approximately 10% at 130 GeV, we assume photons in the 120-140 GeV band to encompass the photons related to the γ-ray line

observation, while photons in the low and high energy bands correspond to background events not associated with the γ-ray line observation. Below, a power-law fit to the sidebands will be used to fix the background rate in our 120-140 GeV simulations while the remainder of the photon excess will make up the signal. We note that there is some evidence for a second line at energies of around 111 GeV [18], however the weak significance of that feature makes its impact on the population of 70-110 GeV γ-rays negligible.

In comparing the photon morphology from the line region against the "side-band" photons, we assume that the background morphology remains approximately invariant throughout the 70-300 GeV energy range. This assumption is warranted in light of observations indicating that the primary component of diffuse emission through this region stems from π^0-emission tracing the Galactic gas [29, 67]. While some unresolved point-sources may also be present, it is unlikely that any given source contributes multiple photons to the observed high-energy γ-ray emission, making the spectral features of each individual source irrelevant.

Before proceeding with the description of the clustering algorithm we employ in this analysis, we describe in the following sections the simulated data sets we use to validate our analysis. Section II B details the simulated line events from both dark matter annihilation scenarios with different dark matter density profiles, and scenarios with one or more point sources. Section II C details the simulated background events. Finally, sec. II D describes the clustering algorithm we employ in the present study.

B. Dark Matter and Pulsars Models

In order to establish a quantitative measure for the clustering properties of γ-rays due to either dark matter or one or more point-sources in the GC region, we produce Monte Carlo simulations of the expected positions of photons stemming from each model.

In the case of PSRs, we examine models featuring between 1 and 6 point sources to explain the excess 130 GeV emission. We randomly pick the distribution of each point source following a surface density distribution $\rho(\mathrm{r}) \propto \mathrm{r}^{-1.2}$, as motivated by the observed density distribution of O/B stars in the inner Galaxy [68] and we produce an excess number of photons which are distributed randomly (assuming equal brightness) between the simulated pulsars.

In the case of dark matter annihilation, we predict the annihilation signal to follow the integral over the line of sight of the square of the dark matter density. We choose two independent dark matter density profiles motivated by models of dark matter structure formation. We first examine a generalized Navarro-Frenk-White [12] profile, with a density profile

$$\rho(r) \propto \left(\frac{r}{r_s}\right)^{-\alpha} \left(1+\frac{r}{r_s}\right)^{-3+\alpha} . \qquad (1)$$

In our standard analysis we choose $\alpha = 1$ and $\mathrm{r}_s = 22$ kpc fitting the best numerical results from the Aquarius simulation [13]. In order to evaluate the effect of changing the dark matter density profile, we also consider an Einasto profile with a density distribution [13]:

$$\rho(r) \propto \exp\left[-\frac{2}{\alpha}\left(\left(\frac{r}{r_s}\right)^{-\alpha} - 1\right)\right], \qquad (2)$$

assuming, here, that $\alpha = 0.17$ [13]. In each case, we assume that the annihilation rate is proportional to $\rho^2(\mathrm{r})$, and then integrate over the line of sight from the solar position $\mathrm{R}_\odot = 8.3$ kpc [69] in order to generate the dark matter morphology that would be observed by the Fermi-LAT.

We additionally consider two alternative profiles. First, the case of decaying dark matter following the NFW profile given in Eq. (1), with the decay rate now proportional to $\rho(\mathrm{r})$. Second, the case of isotropic emission, i.e. a uniform surface profile. Since the clustering properties of the source are highly dependent on the number of observed photons, we calculate for Fermi-LAT (H.E.S.S.-II), 10^5 (2000) realizations of 48 (5000) photons following the distribution assumed in each of these cases over a 10° (4°) square window. For H.E.S.S.-II observations, we estimate the number of photons from a relatively short exposure time, on the order of a 6.25 hours, using an effective area given for the H.E.S.S.-II telescope with the flux in the 130 GeV energy range measured by the Fermi-LAT.

In each case, we must also consider the smearing of target photons based on the point-spread function of the Fermi-LAT telescope. In order to accomplish this accurately for observations at the GC, we employ the Fermi tools to estimate the point-spread function for photons entering both the front and back of the instrument at different θ-angles. Specifically, we employ the *gtpsf* tool developed by the Fermi-LAT collaboration in order to calculate the effective PSF given the total exposure of the GC region from all locations in the Fermi-LAT instrumental phase space (i.e. how much was the GC viewed from different spacecraft orientations). For the selected observation period, the average (68%, 95%) containment radius over the observation is (0.124°,0.529°) for front-converting events ($\sim 56\%$ of exposure area) and (0.258°,0.907°) for rear converting events ($\sim 44\%$ of exposure area). The resulting PSF for each photon (signal and background) is randomly chosen based on this weighted average of instrument coordinates and the incoming photon is smeared based on the given PSF. In the case of Atmospheric Cherenkov Telescope (ACT) simulations, the PSF depends somewhat sensitively on the angle

of incidence of the incoming photons. Following Aharonian *et al* [70] we approximate the H.E.S.S. point-spread function as an energy independent, two-component Gaussian with the probability density of an event smearing to radius θ given by,

$$P(\theta) = A\theta \left[\exp\left(-\frac{\theta^2}{2\sigma_1}\right) + A_{rel} \exp\left(-\frac{\theta^2}{2\sigma_2}\right)\right] \quad (3)$$

Where $\sigma_1 = 0.046$, $\sigma_2 = 0.12$, and $A_{rel} = 0.15$ and an overall normalization A.

C. Background Models

In order to characterize the morphology of the expected diffuse background we follow the detailed PASS 7 Galactic Diffuse Model, which contains both spectral and morphological information generated by observations of both HI and CO line surveys, which constrain the distribution of interstellar gas. The γ-ray morphology and spectrum are then generated by convolving these maps with the modeled cosmic-ray densities utilizing the Galprop code [71], and calculating the expected γ-ray emission from processes including π^0-decay, bremsstrahlung emission, and inverse-Compton scattering. Utilizing these simulations, we then generate a Monte Carlo population of background γ-rays following a morphology compatible with observations across the γ-ray spectrum.

In the case of the Fermi-LAT telescope, we assume zero cosmic-ray contamination, since we are considering only the GC region, which is very bright in γ-rays. Given the calculated intensity of the γ-ray line, we calculate an average of 12 signal, and 36 background photons between an energy of 120–140 GeV. In each simulation of the Fermi-LAT data, we allow the strength of this signal to float using Poisson statistics, setting the mean intensity to be 12 signal photons. For Fermi-LAT observations we model a 10° square window around the GC.

In the case of ACT observations, we note that cosmic-ray contamination is a much larger issue, since hadronic showers dominate the data collected by these telescopes. Extrapolating the cosmic-ray and γ-ray signals from recent low-energy H.E.S.S. observations at 300 GeV [72] and using the best estimates for the H.E.S.S.-II instrumental characteristics [73], we find that 86% of the total background signal will stem from cosmic-ray backgrounds. Thus, for ACT observations we create a simulation composed of 4.35% signal photons, 13.15% diffuse background photons (following the Fermi PASS-7 Galactic diffuse model) and 82.5% isotropic background photons. As in the case of Fermi-LAT observations, we allow the total number of signal photons to float using Poisson statistics, and maintain a background which is 86% isotropic, and 14% diffuse. For H.E.S.S.-II observations we model a 4° square window around the GC, consistent with the smaller field of view of ACT instruments.

The background model described above is also used to estimate the average background count N_b during the computation of the cluster significances. N_b is calculated by integrating the background template, normalized to the correct background count over the 95% containment area of the cluster members (100% containment in cases with fewer than 20 cluster members). This allows for a statistical measure which traces the local morphology of the background and is thus minimally dependent on its anisotropic structure, reducing the significance of 'hot-spots' in the background which may be falsely identified as true clusters.

D. Clustering Algorithm

In order to classify the spatial morphology of photons in a statistically robust way, we employ the *Density Based Spatial Clustering of Applications with Noise* (DBSCAN) algorithm [74], which is capable of both distinguishing cluster points from noise and constraining the maximum connectivity size based on the instrumental point-spread function. DBSCAN possesses two input parameters, corresponding to the assumed radius (ϵ) of each cluster neighborhood and the number of points ($\mathrm{N_{min}}$) which must be contained within a neighborhood to form a new cluster or add to an existing cluster. Our implementation of DBSCAN, modified from the Scikit-Learn `python` package [75], works as follows:

1. For each point in the input list, define the 'ϵ-neighborhood' as a circle of radius ϵ centered on the point of interest.

2. If a point's ϵ-neighborhood contains greater than N_{min} points a new cluster is formed and that point is marked as a 'core point'.

3. Two core points are considered 'density-connected' if the points are mutually contained with in each other's ϵ-neighborhoods. All density connected points are then merged into a single cluster.

4. Require any cluster to contain at least 3 core points.

Traditional DBSCAN implementations also define the notion of 'density reachable' to indicate points which are not themselves density-connected, but which lie within a core point's ϵ-neighborhood. This property is, however, not symmetric, and cluster assignment in general depends on the input ordering of the data. Our algorithm ignores density-reachable points, thus ensuring deterministic results. While we assume, in this analysis, that each profile is centered at the position of the GC, our results are independent of this assumption as the DBSCAN algorithm focuses on the relative position between photons, oblivious to any zero point of the profile. We note that a slightly modified DBSCAN algorithm has already been employed on Fermi-LAT data in the past [76].

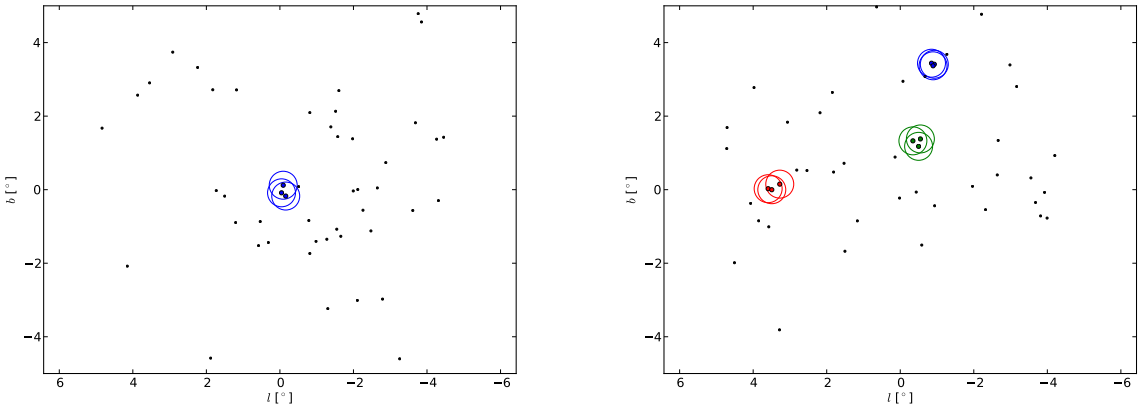

FIG. 1: Event map of Fermi photons between 120-140 GeV (left) and a sample 3 pulsar Monte Carlo simulation (right) showing in colored circles the DBSCAN $\epsilon-$neighborhoods for core points in each detected cluster.

To exemplify the use of the DBSCAN algorithm, Figure 1 shows the DBSCAN analysis of the Fermi-LAT photon events measured with an energy between 120 – 140 GeV (left), and of a simulated model containing two point sources near the galactic center (right). In each case, we show the DBSCAN ϵ-neighborhoods for each core point of each detected cluster. For the Fermi results, DBSCAN finds only one cluster (interestingly centered on the actual Galactic center location!), while in the 3 pulsar simulation case, the algorithm correctly identifies three clusters, at the positions corresponding to where the pulsar photons were generated. The following discussion explains in detail the procedure we employ to apply DBSCAN to γ-ray data.

To quantitatively compare our models against *Fermi* data, we follow Tramacere and Vecchio [76] and employ the likelihood ratio proposed by Li and Ma [77] to calculate the cluster significance, s, in terms of the number of cluster photons N_s and background photons N_b:

$$s = \sqrt{2\left(N_s \ln\left[\frac{2N_s}{N_s+N_b}\right] + N_b \ln\left[\frac{2N_b}{N_s+N_b}\right]\right)} \quad . \quad (4)$$

Here, N_b represents the expected background counts, determined by integrating a diffuse background model (discussed in Subsection II C), while N_s is based on the total photon count contained in the cluster; we effectively adopt $\alpha = 1$ in the notation of Ref. [77]. According to Ref. [77], as long as N_s and N_b are not too sparse, one can equate a cluster with significance s to an "s-standard deviation observation". Thus a cluster significance $s = 2$ implies the cluster is a 2σ fluctuation above the mean background as computed in Subsection II C. We will use this nomenclature in our analysis. With the individual cluster significance in hand, we now define the *"global" significance* S as the mean significance of each detected cluster weighted by the number of photons in that cluster. We then optimize the choices of the DBSCAN parameters ϵ and $N_{\rm min}$ for ACT simulations by maximizing the global significance for the clustering results from our pulsar simulations. Finally we explain why this optimization procedure does not work with the limited Fermi photon count at 130 GeV and choose appropriate DBSCAN parameters based on the Fermi spatial point spread function.

The value of ϵ must be large enough that true cluster elements are not excluded, but small enough that noise is not included. The variable ϵ, as a result, is closely tied to the physical size of the instrumental PSF. One must additionally choose a value $\rm N_{min}$ large enough such that the background does not easily fluctuate above this number, but low enough that one has a high efficiency of finding real clusters. To this end, we use simulations of 1, 2, and 3 pulsar models for Fermi simulations, and 2, 4, and 6 pulsar models for ACT observations to determine a region of $(\epsilon, N_{\rm min})$ parameter space which simultaneously optimizes the significance and detection efficiency. Displayed in the top row of Figure 2 is the global clustering significance (shown in filled contours) and number of detected clusters with $s > 1.29$ (inset, labeled contours) for 48 photon Fermi simulations of 1, 2, and 3 pulsars as a function of the DBSCAN parameters ϵ and $N_{\rm min}$. In the bottom row, we again plot the global clustering significance and number of detected clusters with $s > 2$ for 5000 photon ACT simulations with columns from left to right corresponding to 2, 4, and 6 pulsar models. We note that we apply a firm cut that $N_{\rm min}$ must be at least 3, as this represents the lowest possible non-trivial clustering which may be analyzed by the DBSCAN algorithm.

Inspection of the all three columns for both Fermi and ACT simulations reveals that the clustering algorithm detects clusters at high significance over large coincident regions of DBSCAN parameter space. In the case of ACT observations where the clusters are better differentiated from the background, we also see that these regions also detect the correct number of clusters until the number of

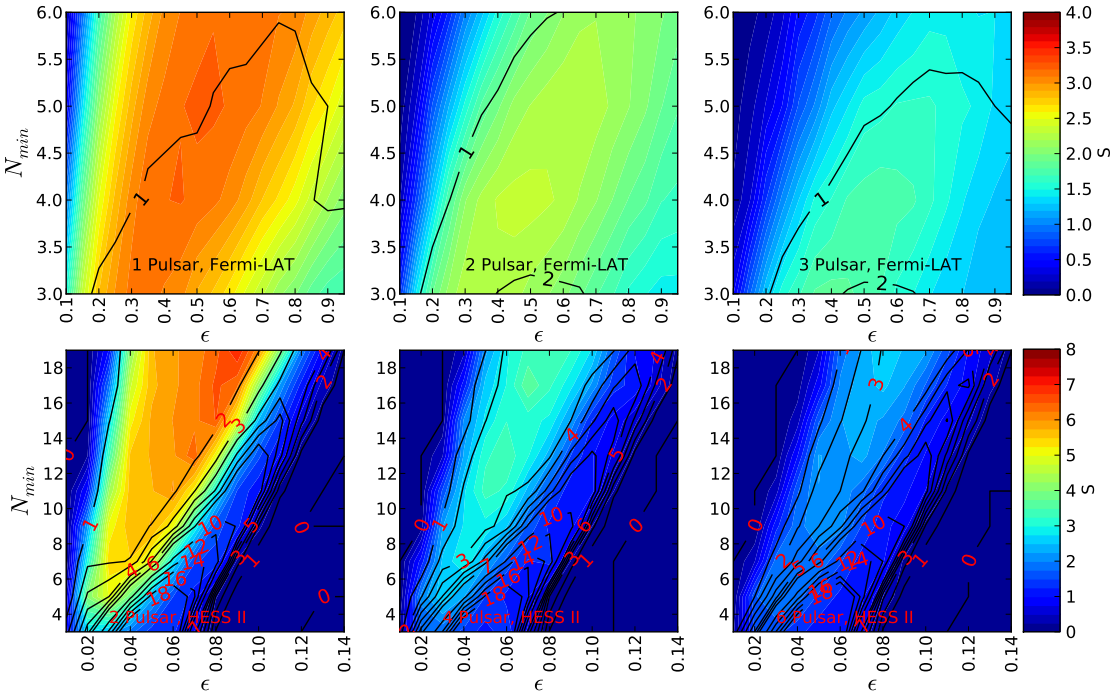

FIG. 2: *Global cluster significance* S (filled colored contours) and *total number of clusters* $N_{\rm clusters}$ for Fermi (ACT) simulations (above threshold $s > 1.29$ ($s > 2.0$); labeled contours) as a function of the DBSCAN search radius ϵ and core-point threshold $N_{\rm min}$. The top row corresponds to Fermi simulations of 1 (left),2 (center), and 3 (right) pulsar models while the bottom row is for ACT observations of 2 (left), 4 (center), and 6 (right) pulsar models. Results are relatively insensitive to large coincident regions in the scan parameter space for left and center columns, while the dependence on $N_{\rm min}$ increases as the number of photons per pulsar approaches the background rate. Fermi simulation DBSCAN parameters are chosen to be $\epsilon = 0.35$, $N_{\rm min} = 3$ while ACT simulation DBSCAN parameters are chosen to be $\epsilon = 0.05$, $N_{\rm min} = 8$ as a compromise between the cluster detection efficiency and the significance over background.

pulsars becomes to large to reliably detect all true clusters. This indicates that the results are robust for most reasonable choices of scan parameters while in the case of 6 pulsars, the number of detected clusters is somewhat more sensitive to parameter choices. For these ACT simulations, we see that choosing $N_{\rm min}$ too small, or ϵ too large can lead to the identification of extra (false) clusters which lowers the overall significance.

We choose our scan parameters based on the 6 pulsar simulations (bottom right) which have the lowest signal to noise ratio among the models we consider here. These considerations motivate a choice of $\epsilon = 0.35°$, $N_{\rm min} = 3$ for Fermi simulations and $\epsilon = 0.05°$, $N_{\rm min} = 8$ for ACT projections as a balance between preserving significance and detecting most of the clusters at $s > 2$. We note that detailed studies on the behavior of DBSCAN settings applied to Fermi-LAT data at lower energies have found qualitatively comparable optimization regions for DBSCAN parameters [76].

In summary, for ACT observations we expect ∼5000 photons for a 6h exposure, and use our significance measure balanced against the number of detected clusters to optimize the DBSCAN parameters. We find $\epsilon = 0.05°$ and $\rm N_{min} = 8$. For Fermi observations, we choose $\epsilon = 0.35°$ and $\rm N_{min} = 3$, which represents the lowest level of non-trivial clustering. We note that there are only 48 photons in our sample, and thus we do not expect to be able to identify more than a few clusters corresponding to point sources with our analysis technique.

III. RESULTS

In order to compare our models of the expected 130 GeV line signal produced by both dark matter and pulsars, we first calculate the clustering properties of the actual Fermi dataset in the energy range of 120-140 GeV using the DBSCAN algorithm. We find only one detected cluster with a significance of $s = 1.29$, an angular scale of 0.22° (defined as the mean pairwise distance of each pair of cluster members), and 3 member photons (see Fig. 1, left).

We first define the parameters useful for differentiating different emission classes and then compare to current

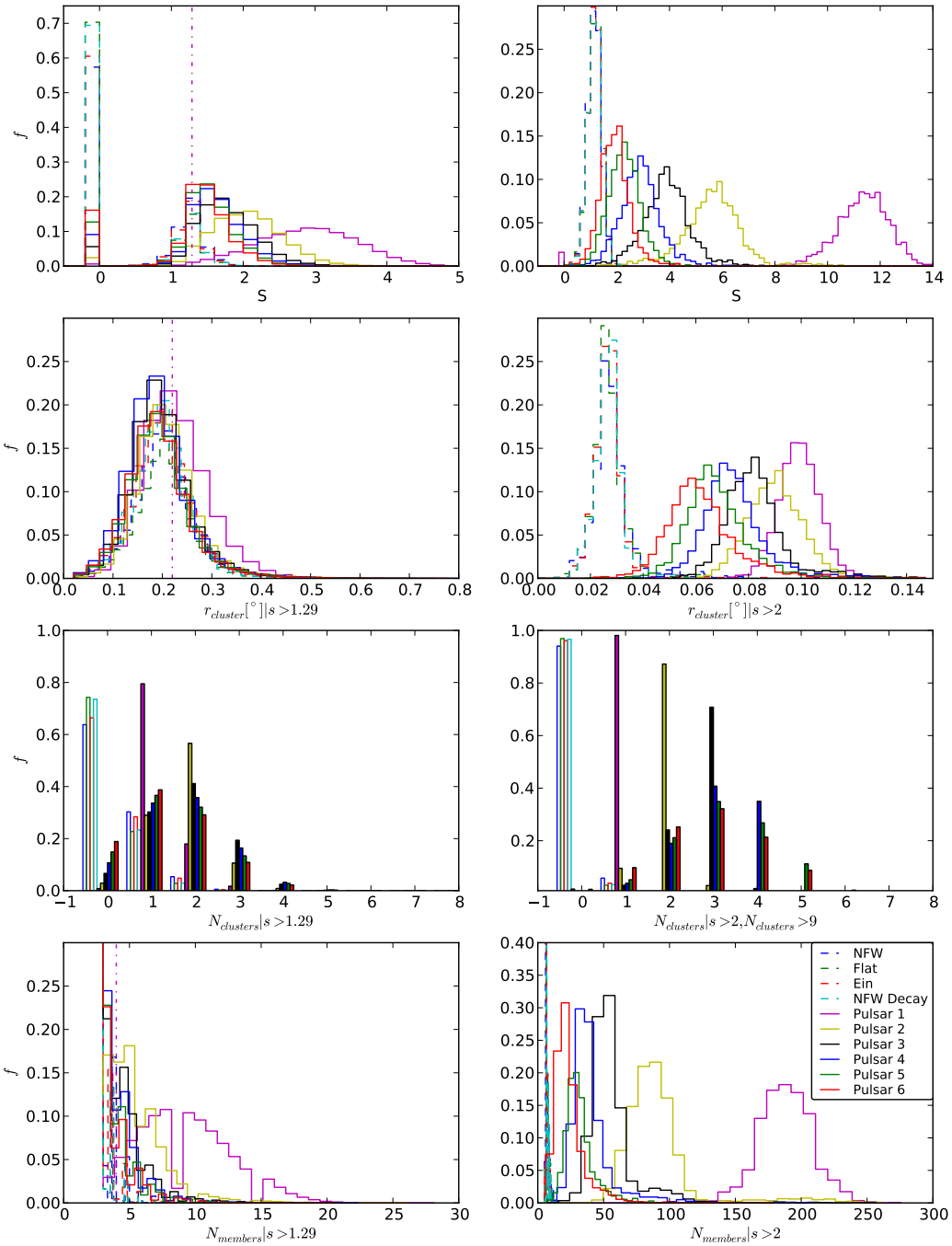

FIG. 3: Models for the clustering properties expected from both Fermi-LAT (48 photons total, left) and H.E.S.S.-II (5000 photons total, right) observations of annihilating dark matter following a NFW profile (blue dashed), flat density profile (green dashed), Einasto profile (red dashed) and decaying dark matter following an NFW profile (cyan dashed), as well as models of emission from undetected groups of one (magenta solid), two (yellow), three (black), four (blue), five (green), and six (red) pulsars, compared to the clustering properties observed in the Fermi-LAT data binned from 120-140 GeV (magenta dot dash). The top row shows the distribution of global significance of detected clusters (S, top row). All other quantities are calculated in the subspace of clusters with significance $s > 1.29$ ($s > 2$) for Fermi (ACT) simulations. Shown is the distribution of *mean clustering radii* (2nd row), the distribution of the *total number of clusters* detected (3rd row), and the distribution of the average *number of member photons* in each cluster with $s > 2$ (bottom).

Fermi data and projections for upcoming H.E.S.S.-II observations. In addition to the global significance, S, we define three quantities in the space of clusters with significance $s > 1.29$ for Fermi and $s > 2$ for ACT observations. The quantities we employ are chosen to best capture the results of each simulation based on the output of DBSCAN, and provide useful information on the clustering properties of each source model. Specifically, we use:

1. the *mean clustering radius*, $r_{\rm cluster}$, defined as the average of the mean pairwise distance (angular scale) of each cluster above threshold, weighted by the cluster's significance;

2. $N_{\rm clusters}$ defined as the *total number of clusters* detected above threshold with at least 3 (10) cluster members for Fermi (ACT), and

3. $N_{\rm members}$ defined as the *mean number of photons* of clusters above threshold, weighted by each cluster's significance. The significance weighting is used simply to suppress the influence of clusters which are likely background fluctuations.

In Figure 3 we show the results of the DBSCAN algorithm applied to both the Fermi data (vertical dashed-dotted line), compared to results from Monte Carlo simulations of dark matter and point source emission from pulsars for 48 photons (left; resembling Fermi-LAT observations) and 5000 photons (right; resembling ACT observations). The dashed lines correspond to diffuse dark matter annihilation models – NFW (blue dashed), Einasto (red dashed), NFW decay model (cyan dashed) and a flat distribution (green dashed). Pulsar models are represented by solid lines – 1 (magenta), 2 (yellow), 3 (black), 4 (blue), 5 (green), and 6 (red). Each histogram is normalized and if no clusters are found, the significance defaults to zero. We thus see that it is much less likely for diffuse models to produce clusters dense enough to be picked up by DBSCAN, indicating that our combination of ϵ and $N_{\rm min}$ are reasonably efficient at rejecting spurious background clusters, especially in the ACT case.

The *global cluster significance* S (top row of Figure 3) provides the strongest metric for differentiating point-source from diffuse emission. Diffuse models should possess virtually identical clustering properties as the extent of any true structure is much larger than the instrumental point spread function. Thus, diffuse sources should only occasionally produce low significance, loosely grouped clusters due to background fluctuations. One possible exception for dark matter models is the identification of a single point source at the GC where the dark matter annihilation rate can be very large. It is notable that the single cluster found in the Fermi data lies precisely on the galactic center. We see in the case of Fermi simulations (top left panel) that there is a fairly sharp cutoff in the fraction of models with global significance $S \lesssim 1$. This lower bound is set by DBSCAN's minimum cluster detection requirements, as well as the location of the cluster with respect to the background template, which determines the number of background photons in that region. Because the cluster detected in the Fermi data is loose, we expect the single detected Fermi cluster to be close to the effective cutoff ($S = 1.29$ for the detected cluster).

Model	$f^{\rm Fermi\text{-}LAT}_{s>1.29}$ $n=1$	$f^{\rm Fermi\text{-}LAT}_{s>1.29}$ $n=2$	$f^{\rm ACT}_{s>2.0}$ $n=1$	$f^{\rm ACT}_{s>2.0}$ $n=2$	$f^{\rm ACT}_{s>2.0}$ $n=3$
NFW	0.362	0.059	0.060	0.002	0.0
Einasto	0.335	0.052	0.039	0.001	0.0
NFW Decay	0.264	0.031	0.034	0.001	0.0
Flat	0.257	0.030	0.031	0.001	0.0
1 Pulsar	0.992	0.197	0.984	0.003	0.0
2 Pulsars	0.971	0.681	0.997	0.902	0.030
3 Pulsars	0.934	0.631	0.998	0.967	0.726
4 Pulsars	0.897	0.556	0.997	0.956	0.769
5 Pulsars	0.851	0.485	0.993	0.942	0.730
6 Pulsars	0.811	0.424	0.985	0.888	0.635

TABLE I: The fraction of simulations with at least 1 cluster of significance $s > 1.29$ ($n = 1$ and $s = 1.29$, corresponding to the maximum n and s_i for clusters i found in Fermi-LAT data) for Fermi-LAT simulations (column 2), the of Fermi-LAT simulations with at least 2 clusters of significance $s > 1.29$ (column 3) and fraction of simulations with at least n clusters detected at significance $s > 2.0$ with at least 10 core points for ACT simulations (columns 4-6).

The second row of Figure 3 shows the *mean clustering radius*. For ACT observations there is a clear division between the point source and smaller diffuse emission scales. However, the Fermi-LAT simulations do not offer any useful discrimination between models with such low photon counts. For point sources, this distribution is governed by the average value of the PSF and possesses an asymmetric tail at larger scales due to the inclusion of background photons and events whose true position is determined by the long PSF tails. For diffuse models, the distribution is governed dominantly by the ϵ DBSCAN parameter until the background density becomes dominant.

Displayed in the third row is the distribution of the *total number of clusters*, $N_{\rm clusters}$, found with significance s > 1.29 (s > 2). In the case of ACT observations we also require clusters to have at least 10 core points to be included whereas we required only 3 for Fermi. We expect to be able to discern *at most* $N_{sig}/N_{\rm min}$ point sources if the signal photons happen to distribute themselves evenly between sources. Even in this case, these true clusters may still lie below the significance threshold. It is realistic to identify only 2-3 true clusters with 12 signal photons (48 total) if they in fact have point source progenitors. This is reflected here. For diffuse sources, only a fraction the detected clusters pass the significance cut. As the number of events is increased, this significance cut could be increased to maintain a high acceptance/rejection ratio, though it is clear that for diffuse models, we typically obtain either zero clusters or one

cluster per simulation with our current significance cuts, while still efficiently detecting several clusters in the case of pulsar models.

Finally, the fourth row contains the distribution of the *mean number of cluster members*, $N_{\rm members}$. For a random distribution of events between pulsars, we expect a Poissonian distribution with a mean of approximately $N_{sig}/N_{pulsars}$ (contributions from the background should typically be <1 photon for Fermi, but the number of signal photons can fluctuate significantly during Poisson sampling). For Fermi-LAT observations we expect 12 ± 3.5 signal photons distributed between $N_{pulsars}$. In the case of ACT observations, we expect 232 ± 15 photons. Occasional spurious clusters will force this distribution downwards, although this effect is reduced by the significance weighting and because we only consider "core points" to be cluster members, thus rejecting those lying on the cluster boundaries.

In order to quantify in how confidently point-source or diffuse models for the 130 GeV excess can be rejected, we count the fraction of simulations which are incompatible with Fermi-LAT data for each tentative source class. A simulation is deemed incompatible if at least 1 cluster is detected at significance $s > 1.29$ corresponding to the maximum number and significance of clusters detected in the Fermi-LAT data. The first column of Table I shows the fraction of simulations for each model with at least one cluster ($n = 1$) with $s_i > 1.29$. In column 3 we show the fraction of simulations which have two clusters detected with a significance of $s_i > 1.29$ in Fermi-LAT simulations, which further demonstrates the vast statistical separations between the clustering properties of diffuse and point-source models. In the subsequent columns we show similar data for the H.E.S.S.-II telescope, which also requires a cluster to have at least 10 core points, and clearly provides an ever greater ability to differentiate between source classes producing the γ-ray line.

Our statistical approach shows that Fermi-LAT data already rule out models where the 130 GeV γ-ray line is produced by 1, (2, 4) or fewer pulsars at the 99% (95%, 90%) confidence level (CL). Specifically, only one cluster was detected in the Fermi-LAT data with a significance $s = 1.29$, while a cluster with a larger significance is observed in more than 90% of simulations with any ensemble of less than 4 point sources. Due to the greatly increased effective area of the H.E.S.S.-II telescope, we find an even greater statistical separation between our models of diffuse and point source emission. This indicates that H.E.S.S.-II will be able to conclusively differentiate models of the 130 GeV line using purely statistical properties.

IV. DISCUSSION AND CONCLUSIONS

If confirmed, the tentative detection of a γ-ray line in the Fermi data might potentially turn into one of the most important breakthroughs on physics beyond the Standard Model, pointing towards the mass of the dark matter particle. Key future developments include the analysis of Fermi γ-ray events with the forthcoming Pass 8 version of the Fermi-LAT analysis software, which will include a major overhaul of the energy reconstruction algorithm [78]. It will also be crucial to identify whether the excess events at 130 GeV from the Earth's limb are indeed a statistical fluke. This question will be answered by increased exposure, which will increase the current statistical sample [18, 28].

At present, barring instrumental effects, a 130 GeV line could be ascribed to either new physics, presumably a dark matter particle decaying or pair-annihilating into a 2γ (or γZ, γh etc.) final state, or to one or more pulsars featuring a cold wind with electrons with an energy at, or very close to, 130 GeV. This latter possibility, it is argued in Aharonian et al. [60], is the only "traditional" astrophysical process envisioned thus far that could produce a sharp gamma-ray line in the energy regime of interest. It is therefore of the utmost importance to discriminate between a cold pulsar wind scenario and a dark matter scenario, if indeed the line is resilient to future tests and observations.

Discriminating dark matter and pulsar interpretations of the 130 GeV line may not be possible based solely on the spectral characteristics of the Fermi-LAT data. In the present study we sought to use morphological information, i.e. the 130 GeV events' arrival direction, to establish whether the signal is likely due to multiple point sources as opposed to a truly diffuse origin. This is a meaningful question, since the signal region is much larger than the instrumental angular resolution, and it should be thus possible to discriminate a finite number of point sources, as expected in the pulsar case, from a distribution that follows a diffuse morphology, such as what expected from dark matter annihilation or decay.

To quantitatively approach the issue of discriminating pulsars versus dark matter on a morphological basis, we employed the DBSCAN algorithm which distinguishes clusters from background noise based on the local photon density. We defined a statistical significance measure, and we optimized the algorithm's two physically well-constrained parameters in order to reconstruct as accurately as possible the potential "clusters" producing the observed γ-ray events.

As a result of our analysis of the available Fermi-LAT data, we concluded that at the 99%, 95%, 90% confidence level the data need at least 2, 3, 5 or more point sources, respectively, while the events' morphology is perfectly consistent with various dark matter density profiles. We conclude that the data strongly disfavor the hypothesis of a small number of pulsars as the origin of the signal. If the pulsar scenario is indeed the culprit for the 130 GeV events, it is necessary to postulate a relatively large population of pulsars (likely at least 4) with cold winds featuring electrons with exactly, to within the instrumental energy resolution, the same energy. This appears, to say the

least, quite problematic. A diffuse origin seems therefore the most likely scenario for the 130 GeV photons. Our clustering algorithm approach, clearly, is not optimized to discriminate between different diffuse morphologies: in fact, on the basis of our results, we find that we cannot discriminate between different diffuse morphologies (like dark matter annihliation vs. decay).

Present and future observatories have the potential to shed additional light on the presence and characteristics of the 130 GeV line [79]. Improvements to the H.E.S.S. telescope (H.E.S.S.-II) have reduced the γ-ray threshold to around 50 GeV, allowing for the independent determination of a line signal from the GC region. This is especially important, as the 10^4 m^2 collecting area of the H.E.S.S. telescope will quickly alleviate the low-statistics issues involved in Fermi-LAT studies [60]. Furthermore, future instruments such as Gamma-400 [80] and CTA [81] are likely to provide the necessary effective area and energy-resolution to definitively and conclusively test the existence and nature the 130 GeV line feature.

However, in the near future, the most important contribution is expected to come from Fermi-LAT itself: Additional data taken since last year, and the continuous accumulation of more data over the next years, will show whether the signature persists or is a rare statistical fluke. Simultaneously, the availability of pass 8 events, based on a set of completely rewritten event reconstruction algorithms for the LAT, will allow a fresh look on possible instrumental systematics.

Acknowledgments

This work is partly supported by NASA grant NNX11AQ10G. SP also acknowledges partial support from the Department of Energy under contract DE-FG02-04ER41286.

[1] W. B. Atwood, A. A. Abdo, M. Ackermann, W. Althouse, B. Anderson, M. Axelsson, L. Baldini, J. Ballet, D. L. Band, G. Barbiellini, et al., ApJ **697**, 1071 (2009), 0902.1089.
[2] F. Yusef-Zadeh, F. Melia, and M. Wardle, Science **287**, 85 (2000).
[3] F. Yusef-Zadeh, W. M. Goss, D. A. Roberts, B. Robinson, and D. A. Frail, ApJ **527**, 172 (1999), arXiv:astro-ph/9907370.
[4] Q. D. Wang, E. V. Gotthelf, and C. C. Lang, Nature **415**, 148 (2002).
[5] K. Ferrière, AAP **540**, A50 (2012), 1201.6031.
[6] R. Schödel, D. Merritt, and A. Eckart, AAP **502**, 91 (2009), 0902.3892.
[7] R. S. Wharton, S. Chatterjee, J. M. Cordes, J. S. Deneva, and T. J. W. Lazio, ApJ **753**, 108 (2012), 1111.4216.
[8] D. Hooper, I. de la Calle Perez, J. Silk, F. Ferrer, and S. Sarkar, JCAP **9**, 002 (2004), arXiv:astro-ph/0404205.
[9] T. Bringmann and C. Weniger, Phys.Dark Univ. **1**, 194 (2012), 1208.5481.
[10] T. Bringmann, X. Huang, A. Ibarra, S. Vogl, and C. Weniger, JCAP **7**, 054 (2012), 1203.1312.
[11] C. Weniger, JCAP **1208**, 007 (2012), 1204.2797.
[12] J. F. Navarro, C. S. Frenk, and S. D. M. White, ApJ **462**, 563 (1996), arXiv:astro-ph/9508025.
[13] V. Springel, J. Wang, M. Vogelsberger, A. Ludlow, A. Jenkins, A. Helmi, J. F. Navarro, C. S. Frenk, and S. D. M. White, MNRAS **391**, 1685 (2008), 0809.0898.
[14] G. R. Blumenthal, S. M. Faber, R. Flores, and J. R. Primack, ApJ **301**, 27 (1986).
[15] O. Y. Gnedin, D. Ceverino, N. Y. Gnedin, A. A. Klypin, A. V. Kravtsov, R. Levine, D. Nagai, and G. Yepes, ArXiv e-prints (2011), 1108.5736.
[16] S. Profumo and T. Linden, JCAP **7**, 011 (2012), 1204.6047.
[17] M. Su, T. R. Slatyer, and D. P. Finkbeiner, ApJ **724**, 1044 (2010), 1005.5480.
[18] M. Su and D. P. Finkbeiner, ArXiv e-prints (2012), 1206.1616.
[19] E. Tempel, A. Hektor, and M. Raidal, ArXiv e-prints (2012), 1205.1045.
[20] R.-Z. Yang, Q. Yuan, L. Feng, Y.-Z. Fan, and J. Chang, Physics Letters B **715**, 285 (2012), 1207.1621.
[21] K. Rao and D. Whiteson (2012), 1210.4934.
[22] M. Kuhlen, J. Guedes, A. Pillepich, P. Madau, and L. Mayer, ArXiv e-prints (2012), 1208.4844.
[23] D. P. Finkbeiner, M. Su, and C. Weniger, ArXiv e-prints (2012), 1209.4562.
[24] A. Hektor, M. Raidal, and E. Tempel (2012), 1209.4548.
[25] A. Boyarsky, D. Malyshev, and O. Ruchayskiy, ArXiv e-prints (2012), 1205.4700.
[26] D. Whiteson, JCAP **11**, 008 (2012), 1208.3677.
[27] D. Whiteson, ArXiv e-prints (2013), 1302.0427.
[28] E. Bloom, E. Charles, E. Izaguirre, A. Snyder, A. Albert, B. Winer, Z. Yang, and R. Essig, ArXiv e-prints (2013), 1303.2733.
[29] D. Hooper and T. Linden, Phys. Rev. D **84**, 123005 (2011), 1110.0006.
[30] A. Rajaraman, T. M. P. Tait, and D. Whiteson, JCAP **9**, 003 (2012), 1205.4723.
[31] B. Shakya, ArXiv e-prints (2012), 1209.2427.
[32] H. M. Lee, M. Park, and W.-I. Park, ArXiv e-prints (2012), 1209.1955.
[33] S. Baek, P. Ko, and E. Senaha, ArXiv e-prints (2012), 1209.1685.
[34] J. Fan and M. Reece, ArXiv e-prints (2012), 1209.1097.
[35] N. Weiner and I. Yavin, ArXiv e-prints (2012), 1209.1093.
[36] L. Wang and X.-F. Han, ArXiv e-prints (2012), 1209.0376.
[37] E. Dudas, Y. Mambrini, S. Pokorski, and A. Romagnoni, ArXiv e-prints (2012), 1205.1520.
[38] M. R. Buckley and D. Hooper, PRD **86**, 043524 (2012), 1205.6811.
[39] K.-Y. Choi and O. Seto, PRD **86**, 043515 (2012),

1205.3276.
[40] L. Bergström, ArXiv e-prints (2012), 1208.6082.
[41] M. Garny, A. Ibarra, and D. Tran, JCAP **8**, 025 (2012), 1205.6783.
[42] Y. Bai and J. Shelton, ArXiv e-prints (2012), 1208.4100.
[43] J. M. Cline, A. R. Frey, and G. D. Moore, ArXiv e-prints (2012), 1208.2685.
[44] T. Li, J. A. Maxin, D. V. Nanopoulos, and J. W. Walker, ArXiv e-prints (2012), 1208.1999.
[45] J. M. Cline, PRD **86**, 015016 (2012), 1205.2688.
[46] S. Tulin, H.-B. Yu, and K. M. Zurek, ArXiv e-prints (2012), 1208.0009.
[47] J.-C. Park and S. C. Park, ArXiv e-prints (2012), 1207.4981.
[48] M. T. Frandsen, U. Haisch, F. Kahlhoefer, P. Mertsch, and K. Schmidt-Hoberg, ArXiv e-prints (2012), 1207.3971.
[49] I. Oda, ArXiv e-prints (2012), 1207.1537.
[50] J. H. Heo and C. S. Kim, ArXiv e-prints (2012), 1207.1341.
[51] T. Cohen, M. Lisanti, T. R. Slatyer, and J. G. Wacker, ArXiv e-prints (2012), 1207.0800.
[52] W. Buchmuller and M. Garny, ArXiv e-prints (2012), 1206.7056.
[53] N. Weiner and I. Yavin, ArXiv e-prints (2012), 1206.2910.
[54] Z. Kang, T. Li, J. Li, and Y. Liu, ArXiv e-prints (2012), 1206.2863.
[55] X. Chu, T. Hambye, T. Scarna, and M. H. G. Tytgat, ArXiv e-prints (2012), 1206.2279.
[56] B. Samir Acharya, G. Kane, P. Kumar, R. Lu, and B. Zheng, ArXiv e-prints (2012), 1205.5789.
[57] H. M. Lee, M. Park, and W.-I. Park, ArXiv e-prints (2012), 1205.4675.
[58] B. Kyae and J.-C. Park, ArXiv e-prints (2012), 1205.4151.
[59] M. Asano, T. Bringmann, G. Sigl, and M. Vollmann (2012), 1211.6739.
[60] F. Aharonian, D. Khangulyan, and D. Malyshev, ArXiv e-prints (2012), 1207.0458.
[61] A. Geringer-Sameth and S. M. Koushiappas, PRD **86**, 021302 (2012), 1206.0796.
[62] A. Hektor, M. Raidal, and E. Tempel, ArXiv e-prints (2012), 1207.4466.
[63] M. Su and D. P. Finkbeiner, ArXiv e-prints (2012), 1207.7060.
[64] D. Hooper and T. Linden, ArXiv e-prints (2012), 1208.0828.
[65] N. Mirabal, ArXiv e-prints (2012), 1208.1693.
[66] C. Weniger, ArXiv e-prints (2012), 1210.3013.
[67] R. Fleysher, in *High Energy Gamma-Ray Astronomy*, edited by F. A. Aharonian, H. J. Völk, and D. Horns (2005), vol. 745 of *American Institute of Physics Conference Series*, pp. 269–274.
[68] R. M. Catchpole, P. A. Whitelock, and I. S. Glass, MNRAS **247**, 479 (1990).
[69] S. Gillessen, F. Eisenhauer, S. Trippe, T. Alexander, R. Genzel, F. Martins, and T. Ott, Astrophys. J. **692**, 1075 (2009), 0810.4674.
[70] R. Cornils, S. Gillessen, I. Jung, W. Hofmann, M. Beilicke, K. Bernlöhr, O. Carrol, S. Elfahem, G. Heinzelmann, G. Hermann, et al., Astroparticle Physics **20**, 129 (2003), arXiv:astro-ph/0308247.
[71] A. Strong, I. Moskalenko, T. Porter, G. Johannesson, E. Orlando, et al. (2009), 0907.0559.
[72] A. Abramowski, F. Acero, F. Aharonian, A. G. Akhperjanian, G. Anton, A. Barnacka, U. Barres de Almeida, A. R. Bazer-Bachi, Y. Becherini, J. Becker, et al., Physical Review Letters **106**, 161301 (2011), 1103.3266.
[73] T. Bringmann, F. Calore, G. Vertongen, and C. Weniger, Phys.Rev. **D84**, 103525 (2011), 1106.1874.
[74] M. Ester, H. peter Kriegel, J. S, and X. Xu (AAAI Press, 1996), pp. 226–231.
[75] F. Pedregosa, G. Varoquaux, A. Gramfort, V. Michel, B. Thirion, O. Grisel, M. Blondel, P. Prettenhofer, R. Weiss, V. Dubourg, et al., Journal of Machine Learning Research **12**, 2825 (2011).
[76] A. Tramacere and C. Vecchio, ArXiv e-prints (2012), 1210.0522.
[77] T.-P. Li and Y.-Q. Ma, ApJ **272**, 317 (1983).
[78] W. Atwood et al. (Collaboration S. Zimmer for the Fermi-LAT) (2013), 1303.3514.
[79] L. Bergström, G. Bertone, J. Conrad, C. Farnier, and C. Weniger, ArXiv e-prints (2012), 1207.6773.
[80] A. M. Galper, O. Adriani, R. L. Aptekar, I. V. Arkhangelskaja, A. I. Arkhangelskiy, M. Boezio, V. Bonvicini, K. A. Boyarchuk, Y. V. Gusakov, M. O. Farber, et al., ArXiv e-prints (2012), 1201.2490.
[81] T. CTA Consortium, ArXiv e-prints (2011), 1111.2183.